LTE Physical-Layer Identity Detection in the Presence of Jamming

Amr El-Keyi[†], Oktay Üreten[‡], Trevor Yensen[‡], and Halim Yanikomeroglu[†]
[†] Department of Systems and Computer Engineering, Carleton University, Ottawa, Ontario.
[‡] Allen-Vanguard Corporation, Ottawa, Ontario.

***Abstract*—In this paper, a novel adaptive physical-layer identity detection algorithm for LTE systems is presented. The proposed algorithm can estimate the location of the primary synchronization signal (PSS) and detect the physical-layer identity in the presence of jamming or interference. Multiple parallel adaptive filters are used to suppress the jamming signal without using any a priori information about its characteristics. Each filter is designed using the linearly constrained minimum variance (LCMV) criterion to minimize the output corresponding to any received signal that does not match the signature of the PSS. The frequency response of the adaptive filters at the PSS timing detection instant is used to suppress the interference/jamming signal during physical-layer identity estimation. Simulation results are presented to illustrate the superior performance of the proposed algorithm compared to earlier non-adaptive PSS detection algorithms.**

***Index Terms*—LTE security, PSS detection, adaptive jamming cancellation, interference mitigation.**

I. Introduction

The Long Term Evolution (LTE) standard has been selected as the technology for implementing several broadband public safety networks, e.g., FirstNet [1]. Recent LTE standards have incorporated a high number of critical technical features and functionalities for public safety operation. Nevertheless, the LTE family is quite vulnerable when it comes to radio security, especially in the presence of a malicious attack or unintended interference [2]. Radio security in LTE, as well as in upcoming 5G standards, is an important concern due to the fact that these "commercial-grade" wireless connectivity technologies will have widespread and highly critical use cases, e.g., intelligent transportation systems, smart cities, and health-care.

Orthogonal frequency division multiplexing (OFDM) has been selected as the modulation technique for the LTE downlink due to its spectral efficiency. One of the major weaknesses of OFDM-based systems is their sensitivity to synchronization errors which can severely degrade the system performance [3]. The effects of partial-band interference on the performance of synchronization algorithms for OFDM systems were studied in [4] where the authors showed that the timing synchronization metric is severely affected by the power of the jamming or interference signal. Jamming attacks against OFDM timing synchronization and signal acquisition can also disrupt LTE-based communication and cause permanent denial of service during the cell selection process [5], [6].

The LTE downlink transmission contains two signals that are broadcasted to enable the user equipment (UE) to synchronize to the system and estimate the cell identity. These signals are the primary synchronization signal (PSS) and the secondary synchronization signal (SSS). Three PSS waveforms are used in LTE that correspond to three possible physical-layer identities. LTE synchronization algorithms start with PSS detection and proceed to SSS detection only after successful identification of the physical-layer identity [7]. Joint PSS detection and identification algorithms search for the peak of the cross-correlation between the received samples and all possible PSS signatures [8]. Reduced complexity PSS detection algorithms that decouple PSS detection and identification were also proposed in [9], [10]. These algorithms exploit the central symmetric-property of PSS signatures or cross-correlate the received signal with the sum of the three PSS signatures. PSS identification can be also performed in the frequency domain by computing the cross-correlation between the discrete Fourier transform (DFT) of the detected PSS sequence and the stored frequency-domain PSS sequences [11].

In this paper, we present an adaptive jamming-resilient PSS detection algorithm for LTE systems that does not require any prior coarse synchronization. The proposed algorithm employs multiple parallel adaptive filters to suppress the jamming signal. The coefficients of each adaptive filter are designed using the linearly constrained minimum variance (LCMV) criterion that minimizes the output power of the filter subject to constraints that preserve the received signal vectors corresponding to PSS signatures only. The coefficients of each adaptive filter are updated iteratively using the recursive least squares (RLS) algorithm. The outputs of the adaptive filters are used to detect the PSS and estimate its location within the LTE downlink frame. The frequency response of the adaptive filters is used to weight the contribution of different subcarriers to the cross-correlation metric in the PSS detection stage. We present numerical simulations that illustrate the ability of the proposed algorithm to effectively eliminate different types of jamming and interference signals and to detect the physical-layer identity of the system even in the presence of carrier frequency synchronization errors. To the best of our knowledge, this is the first paper to consider the design of robust adaptive synchronization algorithms for LTE.

The remainder of this paper is organized as follows. In Section II, we briefly review some relevant features of the synchronization signals broadcasted in the LTE downlink. In Section III, we present the proposed adaptive synchronization algorithm. Our numerical simulations are presented in Section IV. Finally, the paper is concluded in Section V.

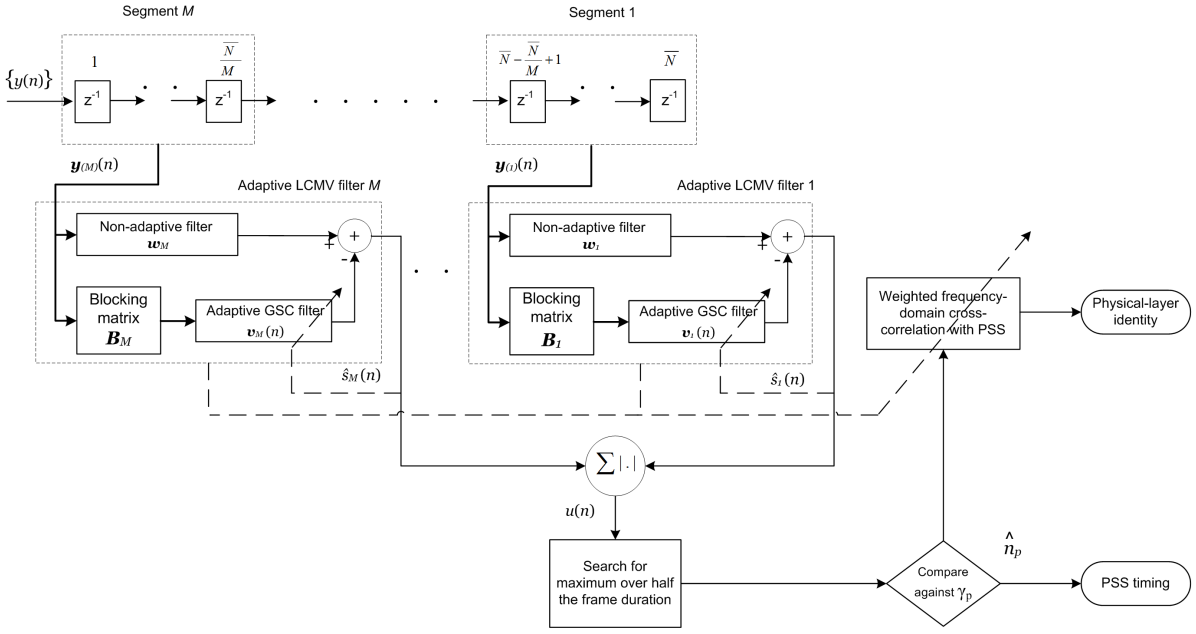

Fig. 1. Block diagram of the proposed adaptive detection algorithm.

II. LTE Downlink Synchronization Signals

LTE downlink transmission is arranged in frames of 10 ms duration. In the frequency division duplex (FDD) mode, each frame is divided into ten subframes and each subframe consists of two slots of duration 0.5 ms each. Each slot in turn consists of a number of OFDM symbols which can be either seven or six based on the CP mode. In the frequency domain, the number of sub-carriers, N, ranges from 128 to 2048, depending on the channel bandwidth. The basic subcarrier spacing is given by 15 KHz and the sampling rate is $f_s = 15N$ KHz. In order to limit the overhead, transmission is scheduled in units of resource blocks (RB). Each RB consists of 12 consecutive sub-carriers and extends over the duration of 1 slot.

The PSS is transmitted twice in each frame. It is located in the last OFDM symbol of the first and 11th slot of each frame. This allows the UE to acquire the slot boundary timing regardless of the CP type. In the frequency domain, the PSS always occupies the central six RBs which allows the UE to synchronize to the network without prior knowledge of its bandwidth. The PSS is constructed from a frequency-domain Zadoff-Chu (ZC) sequence of length 63. Three PSS sequences are used in LTE, corresponding to three physical-layer identities. The selected roots for the three ZC sequences are $r = 25$, 29, and 34 corresponding to physical-layer identities $N_{\mathrm{ID}}^{(2)} = 0$, 1, and 2, respectively. The nth sample of the length-63 ZC sequence with root r is given by

$$\mathrm{P}_r^{63}(n) = \exp\left(-j\frac{\pi rn(n+1)}{63}\right) \quad n = 0, 1, \ldots, 62. \quad (1)$$

Let the $N \times 1$ vector $\boldsymbol{x}_r$ denote the frequency-domain OFDM symbol corresponding to the transmission of the PSS with root index r, i.e., the ith component of $\boldsymbol{x}_r$ contains the information transmitted on subcarrier $i-1$ where $i = 1, \ldots, N$. The vector $\boldsymbol{x}_r$ is given by

$$\boldsymbol{x}_r = [0, \mathrm{P}_r^{63}(32), \ldots, \mathrm{P}_r^{63}(62), \mathbf{0}_{N-63}^T, \mathrm{P}_r^{63}(0), \ldots, \mathrm{P}_r^{63}(30)]^T \quad (2)$$

where $(\cdot)^T$ denotes the transpose operator and $\mathbf{0}_k$ is the $k \times 1$ vector whose entries are all equal to 0. Note that the PSS is transmitted using 62 sub-carriers only where 31 sub-carriers are mapped on each side of the dc sub-carrier. In addition, $\mathrm{P}_r^{63}(31)$ is punctured to avoid modulating the dc subcarrier.

III. Adaptive Detection Algorithm

Fig. 1 shows a block diagram for the proposed algorithm. The algorithm receives a time-domain low-pass filtered signal of bandwidth 480 KHz sampled at $\bar{f}_s \geq 960$ KHz. Since the duration of one OFDM symbol–without the CP–is given by $T = 66.67\mu$s, the number of samples corresponding to one OFDM symbol is given by $\bar{N} = \bar{f}_s T$, i.e., at $\bar{f}_s = 960$ KHz, $\bar{N} = 64$. Recall that the synchronization signals are located on the 62 central subcarriers around the dc subcarrier, and hence, the low-pass filtered input samples contain all the transmitted information in the LTE downlink synchronization signals.

The proposed algorithm can be divided into two stages. In the first stage, M parallel adaptive LCMV filters are used to suppress the jamming signal. The algorithm utilizes the outputs of these filters to detect the location of the PSS within the received LTE downlink signal. In the second stage, the physical-layer identity is estimated by finding the ZC sequence that has the highest "weighted" cross-correlation with the detected PSS sequence in the frequency domain.

A. PSS Detection

Let $y(n)$ denote the nth sample of the time-domain low-pass filtered received signal. Furthermore, let the $\bar{N} \times 1$ vector

$\boldsymbol{y}(n) = [y(n), \ldots, y(n+\bar{N}-1)]^T$ represent the vector containing the latest $\bar{N}$ samples of $\{y(n)\}$ at time instant $n+\bar{N}-1$. The vector $\boldsymbol{y}(n)$ is divided into M segments, $\{\boldsymbol{y}_{(m)}(n)\}_{m=1}^{M}$, each of length $\frac{\bar{N}}{M}$ where

$$\boldsymbol{y}_{(m)}(n) = \left[y\left(n+(m-1)\frac{\bar{N}}{M}\right), \ldots, y\left(n+\frac{m\bar{N}}{M}-1\right)\right]^T. \quad (3)$$

The mth segment of the vector $\boldsymbol{y}(n)$ is linearly processed by the adaptive filter, $\boldsymbol{g}_{(m)}(n)$, to produce the filtered output $s_{(m)}(n)$ which is given by

$$s_{(m)}(n) = \boldsymbol{g}_{(m)}^H(n)\boldsymbol{y}_{(m)}(n) \quad (4)$$

where $(\cdot)^H$ denotes the Hermitian transpose operator and the $\frac{\bar{N}}{M}\times 1$ vector $\boldsymbol{g}_{(m)}(n) = [g_{(m),0}(n), \ldots, g_{(m),\frac{\bar{N}}{M}-1}(n)]^T$ contains the adaptive filter coefficients at time instant n.

The adaptive filters are designed using the LCMV design criterion, i.e., the output power of each filter is minimized while preserving the outputs corresponding to the transmission of any of the three possible PSS signatures. Let the $\bar{N}\times 1$ vector $\boldsymbol{c}_i$ represent the input received signal vector corresponding to transmission of PSS with $N_{\mathrm{ID}}^{(2)} = i$, where $i = 0$, 1, and 2. Furthermore, let $\boldsymbol{c}_{(m),i}$ denote the mth segment of the vector $\boldsymbol{c}_i$. Therefore, the vector $\boldsymbol{g}_{(m)}(n)$ can be obtained by solving the following optimization problem

$$\begin{aligned} \min_{\boldsymbol{g}_{(m)}(n)} \quad & \boldsymbol{g}_{(m)}^H(n)\boldsymbol{R}_{(m)}(n)\boldsymbol{g}_{(m)}(n) \\ \text{subject to} \quad & \boldsymbol{g}_{(m)}^H(n)\boldsymbol{c}_{(m),i} = \frac{1}{M} \qquad \text{for } i = 0,1,2 \end{aligned} \quad (5)$$

where $\boldsymbol{R}_{(m)}(n) = \mathrm{E}\{\boldsymbol{y}_{(m)}(n)\boldsymbol{y}_{(m)}^H(n)\}$ is the covariance matrix of $\boldsymbol{y}_{(m)}(n)$, and $\mathrm{E}\{\cdot\}$ denotes the statistical expectation.

The above LCMV optimization problem can be converted to an equivalent unconstrained optimization problem by using the generalized sidelobe canceller (GSC) decomposition of the adaptive filter coefficients [12]. In particular, let us define the $\frac{\bar{N}}{M}\times 3$ matrix $\boldsymbol{C}_{(m)}$ whose columns contain the mth segment of all the possible PSS signature waveforms, i.e., $\boldsymbol{C}_{(m)} = [\boldsymbol{c}_{(m),0}, \boldsymbol{c}_{(m),1}, \boldsymbol{c}_{(m),2}]$. Let $\boldsymbol{B}_{(m)}$ denote the $\frac{\bar{N}}{M}\times(\frac{\bar{N}}{M}-3)$ matrix whose columns span the nullspace of the columnspace of $\boldsymbol{C}_{(m)}$, i.e., $\boldsymbol{B}_{(m)}^H\boldsymbol{c}_{(m),i} = \boldsymbol{0}_{\frac{\bar{N}}{M}-3}$ for $i = 0$, 1, and 2. Using the matrix $\boldsymbol{B}_{(m)}$, we can decompose the vector $\boldsymbol{g}_{(m)}(n)$ into

$$\boldsymbol{g}_{(m)}(n) = \boldsymbol{w}_{(m)} - \boldsymbol{B}_{(m)}\boldsymbol{v}_{(m)}(n) \quad (6)$$

where

$$\boldsymbol{w}_{(m)} = \frac{1}{M}\boldsymbol{C}_{(m)}\left(\boldsymbol{C}_{(m)}^H\boldsymbol{C}_{(m)}\right)^{-1}\boldsymbol{1}_3 \quad (7)$$

is a fixed weight vector, i.e., independent of n, $\boldsymbol{1}_k$ is the $k\times 1$ vector whose entries are all equal to 1, and the $(\frac{\bar{N}}{M}-3)\times 1$ vector $\boldsymbol{v}_{(m)}(n)$ contains the adaptive GSC filter coefficients at time instant n. By substituting with (6) in (5), we can convert the LCMV problem into the following unconstrained optimization problem

$$\min_{\boldsymbol{v}_{(m)}(n)} \left(\boldsymbol{w}_{(m)} - \boldsymbol{B}_{(m)}\boldsymbol{v}_{(m)}(n)\right)^H \boldsymbol{R}_{(m)}(n)\left(\boldsymbol{w}_{(m)} - \boldsymbol{B}_{(m)}\boldsymbol{v}_{(m)}(n)\right) \quad (8)$$

where the adaptive GSC weight vector that yields the optimal solution of (8) is given by

$$\boldsymbol{v}_{(m)}^{\star}(n) = \left(\boldsymbol{B}_{(m)}^H\boldsymbol{R}_{(m)}(n)\boldsymbol{B}_{(m)}\right)^{-1}\boldsymbol{B}_{(m)}^H\boldsymbol{R}_{(m)}(n)\boldsymbol{w}_{(m)}. \quad (9)$$

Since the covariance matrix $\boldsymbol{R}_{(m)}(n)$ is not readily available at the receiver, we employ the RLS algorithm to estimate the adaptive GSC weight vector iteratively from the received signal samples. The RLS algorithm is initialized by setting the initial weight vector estimate as $\hat{\boldsymbol{v}}_{(m)}(0) = \boldsymbol{0}_{\frac{\bar{N}}{M}-3}$ and its associated covariance matrix as $\boldsymbol{P}_{(m)}(0) = \delta\boldsymbol{I}_{\frac{\bar{N}}{M}-3}$ where $\boldsymbol{I}_k$ denotes the $k\times k$ identity matrix and δ is a large number, e.g., $\delta = 10$. The RLS algorithm employs a forgetting factor λ which gives exponentially less weight to older samples. Given the estimate of the filter coefficients at time instant $n-1$, $\hat{\boldsymbol{v}}_{(m)}(n-1)$, and its associated covariance $\boldsymbol{P}_{(m)}(n-1)$, the RLS algorithm computes the gain vector $\boldsymbol{k}_{(m)}(n)$ as

$$\boldsymbol{k}_{(m)}(n) = \frac{\boldsymbol{P}_{(m)}(n-1)\boldsymbol{B}_{(m)}^H\boldsymbol{y}_{(m)}(n)}{\lambda + \boldsymbol{y}_{(m)}^H(n)\boldsymbol{B}_{(m)}\boldsymbol{P}_{(m)}(n-1)\boldsymbol{B}_{(m)}^H\boldsymbol{y}_{(m)}(n)}. \quad (10)$$

The filter coefficients and the associated covariance are updated respectively by

$$\hat{\boldsymbol{v}}_{(m)}(n) = \hat{\boldsymbol{v}}_{(m)}(n-1) + \boldsymbol{k}_{(m)}(n)\hat{s}_{(m)}^*(n) \quad (11)$$

$$\boldsymbol{P}_{(m)}(n) = \frac{1}{\lambda}\Big(\boldsymbol{P}_{(m)}(n-1) - \boldsymbol{k}_{(m)}(n)\boldsymbol{y}_{(m)}^H(n)\boldsymbol{B}_{(m)}\boldsymbol{P}_{(m)}(n-1)\Big) \quad (12)$$

where $(\cdot)^*$ denotes the complex conjugate operator and $\hat{s}_{(m)}(n)$ is the output of the mth LCMV filter at the nth time instant computed using the estimate of the optimal GSC filter coefficients at time instant $n-1$, i.e.,

$$\hat{s}_{(m)}(n) = \boldsymbol{w}_{(m)}^H\boldsymbol{y}_{(m)}(n) - \hat{\boldsymbol{v}}_{(m)}^H(n-1)\boldsymbol{B}_{(m)}^H\boldsymbol{y}_{(m)}(n). \quad (13)$$

The outputs of the M filters are combined to yield the PSS detection metric $u(n)$ which is given by

$$u(n) = \sum_{m=1}^{M}\left|\hat{s}_{(m)}(n)\right| \quad (14)$$

where $|\cdot|$ denotes the magnitude of a complex number. Due to utilizing the LCMV design criterion, each LCMV filter will suppress its output except when the input corresponds to one of the three possible PSS signatures. As a result, the metric $u(n)$ can be utilized to search for the location of the PSS within the downlink frame. The PSS detection algorithm locates the PSS by searching for the sample index that corresponds to the maximum value of $u(n)$ over half the frame duration, i.e., the search is performed over $5\times 10^{-3}\bar{f}_s$ samples. Let $\hat{n}_P$ denote the samples index corresponding to the maximum value of $u(n)$ over the search window. The proposed algorithm declares detection of the PSS at $n = \hat{n}_P$ if

$$u(\hat{n}_P) \geq \gamma_p \quad (15)$$

where γ_p is a predetermined threshold that can be used to control the probabilities of detection and false alarm.

The number of complex number multiplications required to implement the proposed algorithm in (10)–(13) is given by

$\frac{3\bar{N}^2}{M^2} - \frac{13\bar{N}}{M} + 12$. Since the number of adaptive filters is equal to M, the computational complexity of the adaptive filtering module of the proposed algorithm is of $\mathcal{O}\{\frac{\bar{N}^2}{M}\}$. Increasing the number of segments M reduces the computational complexity at the expense of reduced jamming rejection capability. Recall that the length of each adaptive filter is given by $\frac{\bar{N}}{M}$ and the number of linear constraints in (5) is equal to 3. Hence, each adaptive filter can effectively suppress the jamming signal as long as the rank of its covariance matrix does not exceed $\frac{\bar{N}}{M} - 3$. The effect of the number of segments M on the jamming suppression capability of the proposed algorithm will be illustrated via numerical simulations in Section IV.

In practice, the received signal experiences distortion caused by several radio frequency (RF) mismatches that occur due to the non-ideal characteristics of the devices implemented at the transmitter and/or receiver, e.g., oscillators, mixers, and analog-to-digital and digital-to-analog converters. These RF mismatches cause the received PSS vector to deviate from the ideal PSS signature vector. As a result, the adaptive filters partially suppress the received PSS which reduces the magnitude of the PSS detection metric. For example, in the presence of a carrier frequency offset (CFO) between the transmitter and receiver of magnitude Δf Hz, the components of the received PSS vector experience a progressive phase shift with step $\frac{2\pi\Delta f}{\bar{f}_s}$. Hence, the maximum phase deviation over the length of the PSS signature $\boldsymbol{c}_{(m),i}$ is given by $\frac{2\pi(\frac{\bar{N}}{M}-1)\Delta f}{\bar{f}_s}$. Increasing the number of segments M leads to decreasing the length of the PSS signature waveforms $\boldsymbol{c}_{(m),i}$. As a result, for a given CFO, the distance between the received PSS vector and the subspace containing the protected PSS signature vectors decreases as the number of segments increases. Hence, increasing the number of segments leads to improved robustness against CFO mismatches. The effect of the number of segments on the sensitivity of the proposed algorithm towards CFO will also be investigated via numerical simulations in Section IV.

B. Physical-layer Identity Detection

Since each LCMV filter is designed to have the same output for all possible PSS signatures, the physical-layer identity cannot be directly determined from the outputs of the adaptive filters. Note that due to utilizing the LCMV design criterion, the adaptive filters minimize the output resulting from the contribution of the jamming signal at the PSS detection instant. Let $\boldsymbol{Y}_P = [Y_P(0), \ldots, Y_P(\bar{N}-1)]^T$ denote the $\bar{N}$-point DFT of the received vector at the PSS detection instant, $\boldsymbol{y}(\hat{n}_P)$, i.e.,

$$Y_P(k) = \frac{1}{\sqrt{\bar{N}}} \sum_{n=0}^{\bar{N}-1} y(\hat{n}_P + n) e^{-j\frac{2\pi nk}{\bar{N}}}. \tag{16}$$

Also, let the $\bar{N} \times 1$ vector $\boldsymbol{g}$ denote the concatenation of the adaptive LCMV filters corresponding to the M segments at the PSS detection instant, i.e.,

$$\boldsymbol{g} = \left[\boldsymbol{w}_{(1)}^T - \hat{\boldsymbol{v}}_{(1)}^T(\hat{n}_P)\boldsymbol{B}_{(1)}^T, \ldots, \boldsymbol{w}_{(M)}^T - \hat{\boldsymbol{v}}_{(M)}^T(\hat{n}_P)\boldsymbol{B}_{(M)}^T\right]^T. \tag{17}$$

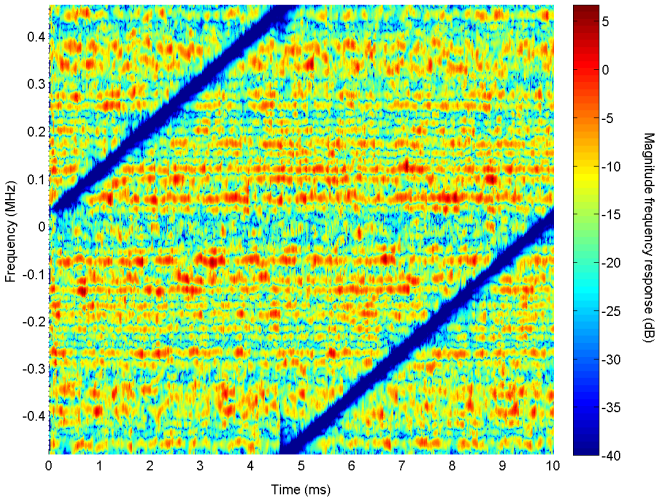

Fig. 2. Magnitude frequency response of the adaptive LCMV filter over the duration of one LTE frame.

Furthermore, let $\boldsymbol{G} = [G(0), \ldots G(\bar{N}-1)]^T$ represent the $\bar{N}$-point DFT of $\boldsymbol{g}^*$. Therefore, the frequency response of the concatenated LCMV filter at the detection instant can be used to suppress the jamming signal to estimate the physical-layer identity. The received PSS symbol on the kth subcarrier after jamming suppression is computed as

$$V(k) = Y_P(k)G(-k). \tag{18}$$

The physical-layer identity can be estimated by computing the cross-correlation between the jamming-free received signal vector at the PSS detection instant and the three PSS signature vectors. However, the PSS signature vectors $\boldsymbol{c}_i$ should be modified to account for the effect of the jamming suppression operation in (18). Let $c_{i,l}$ represent the lth component of the signature vector $\boldsymbol{c}_i$, i.e., $\boldsymbol{c}_i = [c_{i,0}, \ldots c_{i,\bar{N}-1}]^T$. Also, let $\boldsymbol{C}_i = \left[C_i(0), \ldots, C_i(\bar{N}-1)\right]^T$ denote the $\bar{N}$-point DFT of $\boldsymbol{c}_i$, i.e.,

$$C_i(k) = \frac{1}{\sqrt{\bar{N}}} \sum_{n=0}^{\bar{N}-1} c_{i,n} e^{-j\frac{2\pi nk}{\bar{N}}}. \tag{19}$$

The filtered signature sequence of the PSS corresponding to physical-layer identity i is computed as

$$\tilde{C}_i(k) = C_i(k)G(-k). \tag{20}$$

Therefore, the physical-layer identity estimate is given by

$$\hat{N}_{\text{ID}}^{(2)} = \underset{i=0,1,2}{\text{argmax}} \left| \sum_{k=0}^{\bar{N}-1} V^*(k)\tilde{C}_i(k) \right| \tag{21}$$

$$= \underset{i=0,1,2}{\text{argmax}} \left| \sum_{k=0}^{\bar{N}-1} |G(-k)|^2 Y_P^*(k)C_i(k) \right|. \tag{22}$$

The expression in (22) is a weighted frequency-domain cross-correlation of the detected PSS sequence with candidate PSS sequences. The weighting is done using the squared magnitude response of the concatenated LCMV filters at the detection

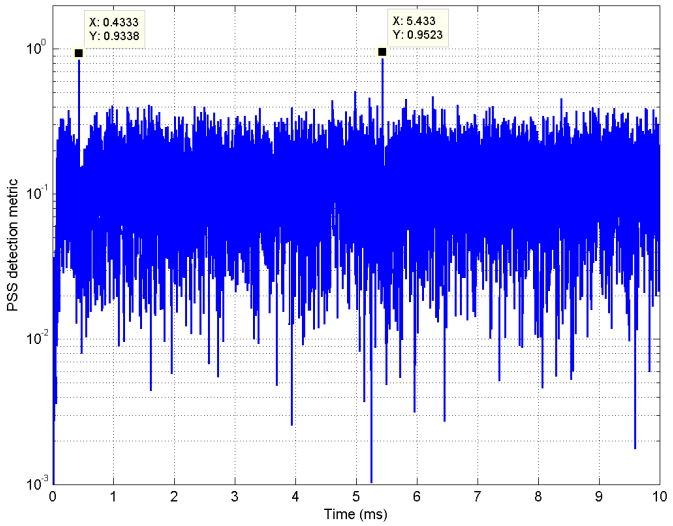

Fig. 3. PSS detection metric versus time.

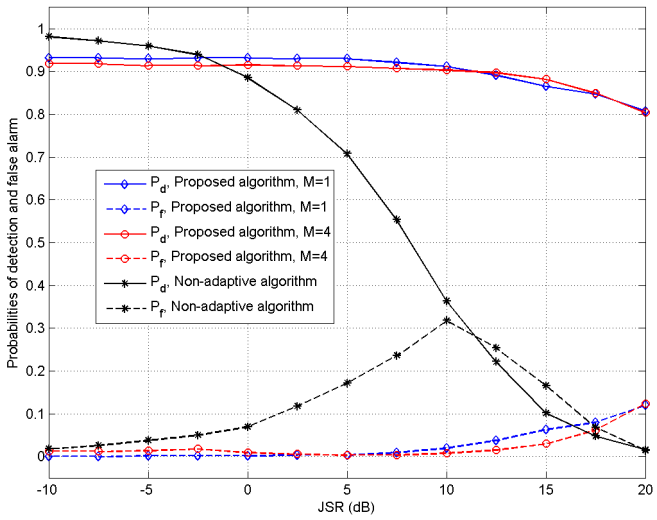

Fig. 4. Probabilities of detection and false alarm versus JSR.

instant in order to reduce the contribution of the jamming signal to the computed cross-correlation metric.

IV. Numerical Simulations

In this section, we investigate the performance of the proposed adaptive synchronization algorithm via numerical simulations. We simulate the downlink of an FDD LTE system with bandwidth 1.25 MHz and normal mode CP. The sampling frequency for the adaptive algorithm is selected as $\bar{f}_s = 960$ KHz resulting in a processing window of length $\bar{N} = 64$. We consider a jamming signal whose frequency chirps linearly from -480 KHz to 480 KHz in a time interval of duration 10 ms. The jamming signal is present over the entire frame duration and the jamming-to-signal (JSR) ratio is set to 20 dB. The parameters of the algorithm are selected as $M = 1$, $\lambda = 0.98$, and $\delta = 10$. In order to focus on illustrating the performance of the PSS detection algorithm, we consider a frequency-nonselective channel. Fig. 2 shows the magnitude response of the adaptive LCMV filter over the temporal duration of one LTE frame. We can see from this figure that the proposed algorithm can effectively track the jamming signal by placing deep nulls at its spectral components. Fig. 3 shows the PSS detection metric, $u(n)$, versus time over the duration of one frame. We can see from this figure that the metric has two clear peaks that are spaced 5 ms apart. The two peaks correspond to the locations of the PSS within the LTE frame. We can also notice from Fig. 3 that the proposed algorithm can effectively suppress the jamming signal and that the peak-to-side-peak ratio is around 2.

We compare the performance of the proposed algorithm to that of a non-adaptive PSS detection algorithm that employs time-domain cross-correlation with the stored PSS signature vectors to detect the PSS location and estimate the physical-layer identity. We investigate the performance of the tested algorithms in the "Extended Pedestrian A" channel model with 5 Hz Doppler (EPA5). Simulation results are obtained by averaging over 500 Monte Carlo runs. In each run, the physical-layer identity is generated randomly. We consider the synchronization algorithm successful if the estimated physical-layer identity is correct and the PSS timing error does not exceed half the length of the CP. On the other hand, a false alarm event occurs when any of the previous conditions is violated given that the threshold γ_p was crossed during PSS search where $\gamma_p = 0.2$ is used in our simulations. Fig. 4 shows the probability of detection, P_d, and the probability of false alarm, P_f for different algorithms versus JSR. We can see from this figure that the proposed algorithm maintains a high probability of detection even in the presence of strong jamming. On the other hand, the performance of the non-adaptive synchronization algorithm starts to deteriorate when the JSR is over 0 dB. We can also notice that increasing the number of segments from $M = 1$ to $M = 4$ causes a slight degradation in the jamming rejection capability of the proposed algorithm.

Next, we investigate the sensitivity of the proposed algorithm to carrier frequency offset (CFO). As discussed earlier, increasing the value of the CFO causes the received PSS vector to deviate more from the ideal PSS signature vector, and hence, the adaptive filter tends to suppress the received PSS instead of preserving it. Fig. 5 shows the probabilities of detection and false alarm of the proposed algorithm for different values of M versus the CFO at JSR=10 dB. We can see from this figure that increasing the number of segments from $M = 1$ to $M = 4$ improves the robustness of the algorithm towards CFO. It is worth mentioning that the same effect was reported in the segmented implementation of the cross-correlation-based PSS detection algorithm in [13].

In order to investigate the effect of the number of segments M on the jamming suppression capability of the proposed algorithm, we consider stationary jamming signals of various bandwidths. Each jamming signal is created as the sum of single tones with 15 KHz spacing starting from $f_{\min}$ to

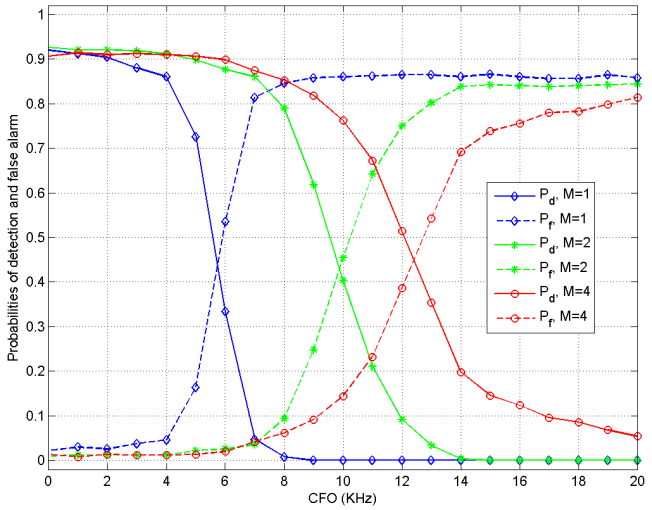

Fig. 5. Probabilities of detection and false alarm versus CFO.

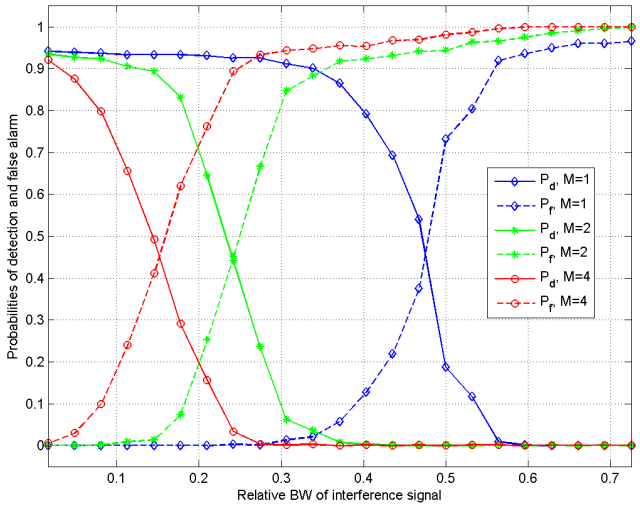

Fig. 6. Probabilities of detection and false alarm versus $\mathrm{BW_r}$.

$f_{\max} = 390$ KHz. We define the relative bandwidth of the jamming signal as

$$\mathrm{BW_r} \triangleq \frac{\left(f_{\max} - f_{\min} + 15 \times 10^3\right)}{62 \times 15 \times 10^3} \tag{23}$$

which represents the fraction of PSS subcarriers affected by jamming. Fig. 6 shows the probabilities of detection and false alarm versus the relative BW of the jamming signal at JSR= 20 dB. We can see from this figure that the proposed algorithm with $M = 1$ can effectively suppress the jamming signal even when it spans one third of the BW of the PSS. When the jamming signal is distributed over more than one third of the BW, the proposed synchronization algorithm cannot effectively cancel the jamming signal while preserving the information contained in the PSS. We can also notice from Fig. 6 that doubling the number of segments from $M = 1$ to $M = 2$ (and from $M = 2$ to $M = 4$) reduces the jamming suppression capability of the proposed algorithm by a factor of two. This can be attributed to the reduced length of the adaptive filters that leads to reducing the available degrees of freedom required to place nulls at the frequencies of the jamming signal.

V. Conclusion

We have presented a robust physical-layer identity detection algorithm for LTE systems that can eliminate jamming signals via adaptive filtering. The adaptive filtering coefficients are designed according to the LCMV design criterion and are updated iteratively using the RLS algorithm. The proposed algorithm utilizes weighted frequency-domain correlation with stored PSS signature waveforms to detect the physical-layer cell identity. Simulation results have been presented that illustrate the superior performance of the proposed algorithm compared to earlier non-adaptive algorithms. The proposed algorithm was shown to be able to successfully detect and identify the PSS even in the presence of strong jamming or interference and large CFO mismatches.

References

[1] A. Paulson and T. Schwengler, "A review of public safety communications, from LMR to voice over LTE (VoLTE)," in *IEEE Symposium on Personal, Indoor, and Mobile Radio Communications*, London, United Kingdom, September 2013, pp. 3513–3517.

[2] C. Shahriar, M. La Pan, M. Lichtman, T. C. Clancy, R. McGwier, R. Tandon, S. Sodagari, and J. H. Reed, "Phy-layer resiliency in OFDM communications: A tutorial," *IEEE Communications Surveys & Tutorials*, vol. 17, no. 1, pp. 292–314, First quarter 2015.

[3] H. Minn, V. K. Bhargava, and K. B. Letaief, "A robust timing and frequency synchronization for OFDM systems," *IEEE Transactions on Wireless Communications*, vol. 2, no. 4, pp. 822–839, July 2003.

[4] M. Marey and H. Steendam, "Analysis of the narrowband interference effect on OFDM timing synchronization," *IEEE Transactions on Signal Processing*, vol. 55, no. 9, pp. 4558–4566, September 2007.

[5] M. J. L. Pan, T. C. Clancy, and R. W. McGwier, "Jamming attacks against OFDM timing synchronization and signal acquisition," in *IEEE Military Communications Conference*, Orlando, FL, October 2012, pp. 1–7.

[6] M. Labib, V. Marojevic, J. H. Reed, and A. I. Zaghloul, "How to enhance the immunity of LTE systems against RF spoofing," in *International Conference on Computing, Networking and Communications*, Kauai, HI, February 2016, pp. 1–5.

[7] Y. Yu and Q. Zhu, "A novel time synchronization for 3GPP LTE cell search," in *International ICST Conference on Communications and Networking in China*, Guilin, China, August 2013, pp. 328–331.

[8] X. Yang, Y. Xiong, G. Jia, W. Fang, and X. Zheng, "PSS based time synchronization for 3GPP LTE downlink receivers," in *IEEE International Conference on Communication Technology*, Jinan, China, September 2011, pp. 930–933.

[9] Z. Zhang, J. Liu, and K. Long, "Low-complexity cell search with fast PSS identification in LTE," *IEEE Transactions on Vehicular Technology*, vol. 61, no. 4, pp. 1719–1729, May 2012.

[10] Y. Gao, G. Zhu, X. Chen, D. Wu, and B. Ban, "A modified algorithm of synchronization signal detection for LTE initial cell search," in *International ICST Conference on Communications and Networking in China*, Harbin, China, August 2011, pp. 1211–1215.

[11] K. Manolakis, D. M. G. Estevez, V. Jungnickel, W. Xu, and C. Drewes, "A closed concept for synchronization and cell search in 3GPP LTE systems," in *IEEE Wireless Communications and Networking Conference*, Budapest, Hungary, April 2009, pp. 1–6.

[12] B. R. Breed and J. Strauss, "A short proof of the equivalence of LCMV and GSC beamforming," *IEEE Signal Processing Letters*, vol. 9, no. 6, pp. 168–169, June 2002.

[13] S. Tang, K. Peng, K. Gong, J. Song, C. Pan, and Z. Yang, "Robust frame synchronization for Chinese DTTB system," *IEEE Transactions on Broadcasting*, vol. 54, no. 1, pp. 152–158, March 2008.